Science of the Total Environment 703 (2020) 135605

Contents lists available at ScienceDirect

Science of the Total Environment

journal homepage: www.elsevier.com/locate/scitotenv

# Towards more sustainable brine extraction in salt flats: Learning from the Salar de Atacama

M.A. Marazuela [a,b,c,*], E. Vázquez-Suñé [a], C. Ayora [a], A. García-Gil [d]

[a] Institute of Environmental Assessment and Water Research (IDAEA), CSIC, Jordi Girona 18, 08034 Barcelona, Spain
[b] Department of Civil and Environmental Engineering, Technical University of Catalonia (UPC), Jordi Girona 1-3, 08034 Barcelona, Spain
[c] Associated Unit: Hydrogeology Group (UPC-CSIC), 08034 Barcelona, Spain
[d] Geological and Mining Institute of Spain (IGME), Manuel Lasala 44, 9° B, 50006 Zaragoza, Spain

## HIGHLIGHTS

- A methodology to characterize the evaporation discharge in salt flats is proposed.
- The water table drawdown caused by Li-rich brine exploitation is evaluated.
- An exponential curve relating phreatic evaporation to water table depth is obtained.
- The impact on the evaporation discharge by brine pumping is quantified.
- A more ecologically efficient design of brine pumping is reported.

## GRAPHICAL ABSTRACT

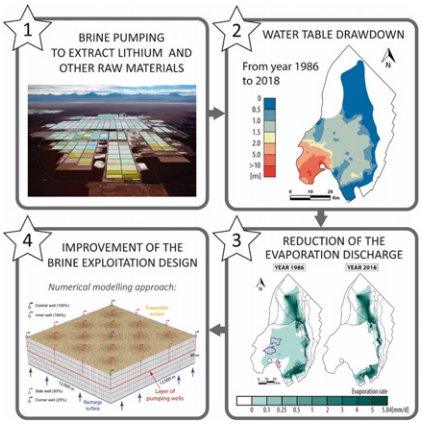


## ARTICLE INFO

*Article history:*
Received 20 September 2019
Received in revised form 16 November 2019
Accepted 16 November 2019
Available online 18 November 2019

Editor: Damia Barcelo

*Keywords:*
Evaporation
Water table
Water balance
Numerical modelling
Pumping
Mining

## ABSTRACT

Salt flats are hydrogeological systems with highly valuable wetland and lake ecosystems. The brine pumping carried out to extract lithium is modifying the natural evaporation discharge of salt flats. A methodology to evaluate the impacts caused on water table and evaporation discharge by brine exploitation in salt flats is proposed and applied to the Salar de Atacama. The methodology included field measurements of water table and evaporation rate, followed by its spatio-temporal analysis and the application of the results to a numerical model to improve the brine exploitation design.

The spatio-temporal analysis of the water table depth and evaporation rates measured in the field concluded that the evaporation discharge decreased from 12.85 to 10.95 $m^3 \cdot s^{-1}$ between 1986 and 2018, that is around 15%. This reduction compensated part of the extractions and could contribute to the preservation of the mixing zone ecosystems. At present, this damping capacity is already amortized in the nucleus and the marginal zone is beginning to be affected by the brine pumping. The sensitivity of the phreatic evaporation on the water table depth justified the great uncertainty of the previous evaporation discharge estimations. Thus, an average error lower than 0.5 m was enough to modify the evaporation by >60%. Therefore, considerable effort should invested to faithfully quantify the discharge by evaporation which is critical in water balance of salt flat basins.

* Corresponding author at: Department of Civil and Environmental Engineering, Technical University of Catalonia (UPC), Jordi Girona 1-3, 08034 Barcelona, Spain.
*E-mail address:* mamarazuela@outlook.com (M.A. Marazuela).

https://doi.org/10.1016/j.scitotenv.2019.135605
0048-9697/© 2019 Elsevier B.V. All rights reserved.

The numerical model pointed out that the total pumping outflow should be distributed in the largest possible area. This minimizes the water table drawdown and maximizes the capacity of the evaporation decline to compensate the extractions. The results of this work serve as guidelines to improve the efficiency of future salt flat exploitations.

© 2019 Elsevier B.V. All rights reserved.

## 1. Introduction

Salt flats are zones of discharge by phreatic evaporation often located in arid to hyperarid climates. Long-term evaporation has allowed the accumulation of a large thicknesses of evaporite rocks and has enriched pore brines in lithium, potassium, boron, iodine and nitrates (Corenthal et al., 2016; Risacher et al., 2003; Warren, 2010; Yechieli and Wood, 2002). These brines contain essential raw materials for batteries, fertilizers and detergents among others (Evans, 1978; Hardie, 1991; Kesler et al., 2012; Lowenstein and Risacher, 2009; Rissmann et al., 2015). The brine is pumped and then transported to evaporation pools where is progressively concentrated until the salts of interest precipitate (Flexer et al., 2018).

The shallow water table favours salt flats usually harbour lake and wetland ecosystem recognized worldwide for their uniqueness. However, the ecological richness of these sensitive ecosystems can be affected by brine pumping as a consequence of the reduction in the discharge by evaporation that causes the drawdown of the water table (Acosta and Custodio, 2008; Scheihing and Tröger, 2018). The free water surface evaporation occurs from lakes and the phreatic evaporation takes place from the shallow water table of salt flats as a function of the water table depth (Philip, 1957). Thus, the increase in thickness of the unsaturated zone caused by brine pumping breaks the natural water balance of the basin (Marazuela et al., 2019b). In addition to the pumped outflow and the hydraulic parameters that are characteristic of each salt flat (Houston et al., 2011), the distribution of the pumping wells is the factor that determines the spatio-temporal evolution of these impacts.

Until now, concessions made by public authorities to mining companies almost always establish limits in terms of the maximum volume of brine that can be extracted. The design of the operation, that is, the distribution of pumping wells, is not usually considered and is ultimately based on the interests of the mining company. Thus, it is of great importance to advance the knowledge of the impacts that brine pumping induces in the evaporation discharge of salt flats to establish the most efficient designs for brine exploitation in terms of ecological impact.

The Salar de Atacama, which is the third largest salt flat globally and it is located in the Central Andean Range (Northeast of Chile), was chosen as a case study to evaluate the impacts caused by brine pumping on the water table and evaporation discharge of salt flats, since it is the best known from the hydrogeological point of view favoured by its outstanding ecosystems and the intense mining pressure carried out to extract Li-rich brines worldwide (Ide and Kunasz, 1990; Kesler et al., 2012; Liu et al., 2019; Munk et al., 2016).

The hydrodynamics of the Salar de Atacama was stablished under natural and anthropogenic regimes (Marazuela et al., 2019a and 2019b). In this endorheic basin, the main recharge occurs by infiltration of rainfall in the eastern volcanic arc and the discharge is produced by phreatic evaporation in the marginal zone and salt flat nucleus. The marginal zone matches the saline interface and its mixing zone which results from the density contrast between the laterally recharged freshwater and the evaporated brine of the nucleus (Boutt et al., 2016; Marazuela et al., 2018; Tejeda et al., 2003). Because rainfall recharge can be considered undisturbed by the effects of mining, the focus in terms of brine pumping impacts on the water balance should be the evaporation rate. Evaporation occurs mainly from the water table, which is very close to the land surface and tends to rise by capillarity (Grilli, 1985; Grilli and Vidal, 1986; Houston, 2006; Kampf et al., 2005; Kampf and Tyler, 2006; Muñoz-Pardo et al., 2004).

The evaporation discharge of the Salar de Atacama has been widely discussed during the last decades. Mardones (1986) quantified the evaporation discharge as 5.29 $m^3 \cdot s^{-1}$. Some subsequent manuscripts and technical reports have used this estimation as a reference what has led them to calculate evaporation discharge in the range of 5.17–5.58 $m^3 \cdot s^{-1}$ (Dirección General de Aguas, 2013, 2010, 1986; Muñoz-Pardo et al., 2004). Kampf and Tyler (2006) obtained values of evaporation in a range of 1.60–22.7 $m^3 \cdot s^{-1}$, depending on the multiple calculation methods that were applied, which were based on remote sensing and evaporation zoning. The last quantification established the natural evaporation discharge in 14.90 $m^3 \cdot s$ (Marazuela et al., 2019a). Establishing a methodology for estimating evaporation discharge in salt flats and analysing the sensitivity of its uncertainties is, therefore, necessary.

Furthermore, as the evaporation discharge depends on the water table depth and backwards, salt flats have a damping capacity of water balance that makes very complex to predict the impact generated by the pumping. Any natural or anthropogenic perturbation of the water table causes a change in the evaporation discharge in the opposite direction of the perturbation.

The objectives of this work are (1) to establish a methodology for the estimation of the evaporation discharge in salt flats and to evaluate its sensitivity to the accuracy of the water table depth data, (2) to quantify the spatio-temporal impacts of the brine pumping in the Salar de Atacama case of study and 3) to evaluate the best distribution of brine pumping wells to reduce the ecological impacts on salt flats.

The workflow of the methodology followed to reach these objectives included (1) field measurements of water table depth and evaporation rate (lysimeters and evaporation trays), (2) spatio-temporal analysis of the field data and (3) the application of the knowledge acquired to a numerical model that allows to evaluate the ecological efficiency of brine exploitations (Fig. 1). The spatio-temporal analysis was performed for two extreme snapshots of the Salar de Atacama case study: the natural regime prior to brine pumping (year 1986) and (2) the present regime under intensive brine pumping (year 2018). First, the drawdown caused in the water table by brine pumping was quantified. Second, the distribution of evaporation rates in the whole basin and the subsequent reduction in evaporation discharge were estimated.

## 2. Material and methods

### 2.1. Hydrogeological setting

The Salar de Atacama is located in the Central Andean Range within the Antofagasta Region (Chile), 55 km south of San Pedro de Atacama and 315 km northeast of Antofagasta (Fig. 2). The overall shape of the basin has the long axis in the N-S direction and an area of approximately 17,000 $km^2$. From the centre to the boundary of the basin, four subdomains can be distinguished: the salt flat nucleus, the marginal zone or mixing zone, the alluvial sub-domain, and the basement and volcanic rocks.

The Andean Range suffered numerous tectonic phases that have generated reliefs controlled by faults and folds at local and regional scales and depocenters where many of the Andean salt flats developed (González et al., 2009). The Salar de Atacama basin was subjected to an extensive phase during the Oligocene-Lower Miocene, which was

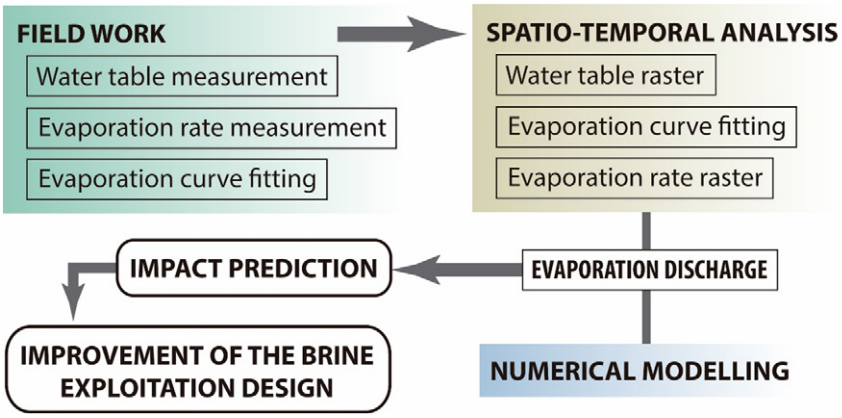


**Fig. 1.** Flowchart of the methodology proposed to assess the evaporation discharge in salt flats and improve the ecological management of brine exploitations.

followed by a compressive phase that is still ongoing (Arriagada et al., 2006). The basin is delimited by inverse faults that affect the rocks of Palaeozoic age that constitute the basement of the current cover (Jordan et al., 2007). The space generated by the movements of these faults has controlled the deposition of filling materials, including the Vilama Formation which constitutes the nucleus of the Salar de Atacama

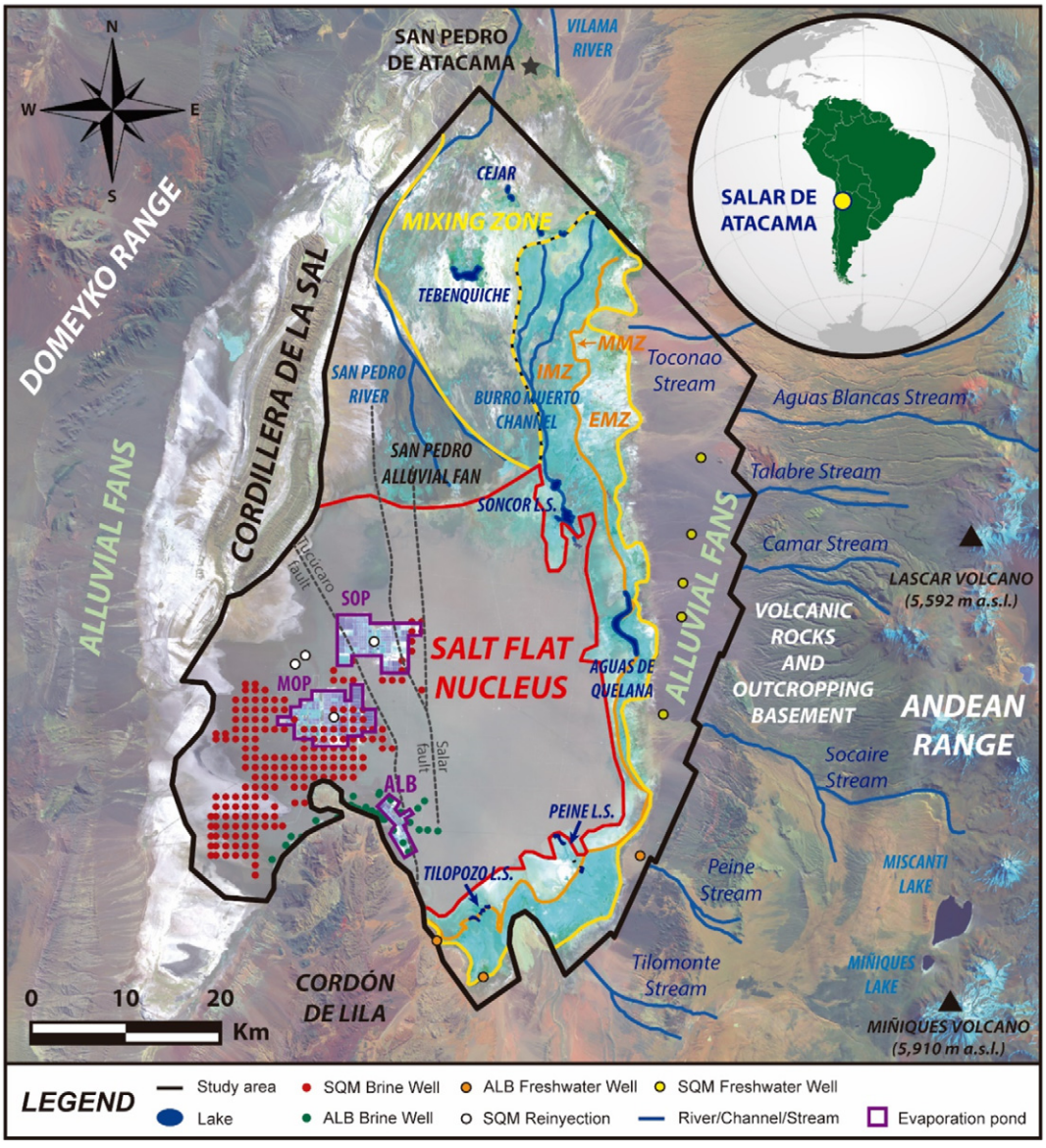


**Fig. 2.** Location of the Salar de Atacama (LANDSAT 8: 27 September 2016). The three sub-zones of the mixing zone are indicated by orange lettering (internal, IMZ; middle, MMZ and external, EMZ, mixing zone).

(>2300 m a.s.l., metres above sea level) (Muñoz et al., 2002). The geometry of the layers is strongly affected by the Salar and Tucúcaro Fault Systems, which make the eastern block of the salt flat nucleus reach a thickness of approximately 1400 m against the only 500 m thickness of the western block (Fig. 3).

The salt flat nucleus is mainly composed by halite. The deposits that border the salt flat nucleus and that are associated with the mixing zone are composed of carbonates and gypsum according to the precipitation sequence by evaporation (Vásquez et al., 2013). The most external zone of the basin is composed of the basement and the volcanic rocks of the current volcanic arc (>5500 m a.s.l.) (González et al., 2009). Previous works have reported a strong variability of the soil characteristics that may condition the evaporation process. Kampf and Tyler (2006) defined the crust of the nucleus as rough halite crust while the crust of the mixing zone was identified as moderately rough crust ranging between soft and hard.

The precipitation reaches >120 mm·yr$^{-1}$ in the volcanic arc and it is reduced to <10 mm·yr$^{-1}$ in the salt flat nucleus (Marazuela et al., 2019a). The saline interface (mixing zone) located in the marginal zone isolates the hydrodynamics of the system in two environments: the salt flat nucleus and the recharge area. The salt flat nucleus acts as a quasi-isolated area, similar to a pool with very slow flows driven by density contrasts. The groundwater flows coming from the eastern mountains conducted by potentiometric gradients converges with the convection cell of the salt flat nucleus and push the groundwater to the surface feeding the lakes of the marginal zone (Marazuela et al., 2019a). Thus, the maximum evaporation rates are reached in the marginal zone where the water table is at the minimum depth in the study area. Three zones inside of the mixing zone were differentiated based on hydrodynamics by Marazuela et al. (2018): the internal mixing zone (IMZ), middle mixing zone (MMZ) and external mixing zone (EMZ) (Fig. 2). The lake systems Aguas de Quelana, Peine (Salada and Saladita Lakes) and Tilopozo (La Punta and La Brava Lakes) are located in the MMZ associated with the main upward groundwater flows. A special case is the Soncor Lake System (Barros Negros, Chaxa and Puilar Lakes) because it is located in the IMZ, and different sources of groundwater and surface water contribute to maintaining its water level (Ortiz et al., 2014).

During the natural regime, prior to brine pumping, the water balance of the basin was established as 14.9 m$^3$·s$^{-1}$, which was approximately equal for the recharge and evaporation (Marazuela et al., 2019a). However, the natural regime has been perturbed by brine pumping. The exploitation of the lithium and other raw materials in the Salar de Atacama is carried out by means of pumping along a very dense network of wells. Several hundred of wells are drilled in the Salar de Atacama at present. The brine pumping was started in 1984 by the Albermale Company (ALB), and since 1994 the Sociedad Química y Minera de Chile (SQM) Company has also conducted brine pumping in the area (Fig. 4) (IDAEA-CSIC, 2017). The mining plants MOP and SOP (Fig. 2), both of which belonged to SQM, began to pump in 1994 and 1996, respectively. Before 1994, the volume of brine pumped did not exceed 0.05 m$^3$·s$^{-1}$; however, from 1994 to 2009, the pumped rates reached values between 0.5 and 1 m$^3$·s$^{-1}$, and from 2010 to the present, they have exceeded 1.5 m$^3$·s$^{-1}$, with a greater increase expected in the coming years that will reach to values higher than 2 m$^3$·s$^{-1}$.

### 2.2. Measurement of evaporation rates

The estimation of the evaporation rate required two different approaches depending on the type of evaporation, i.e., evaporation from free water surface or phreatic evaporation. The first type of evaporation occurs in areas occupied by water bodies open directly to the atmosphere. This type of evaporation occurs in the perennial lakes located in the marginal zone and extends a total area of 3.57 km$^2$. In the remaining areas of the mixing zone and in the nucleus, the main responsible for the groundwater discharge is the phreatic evaporation favoured by the shallow water table.

The rates of both, free water surface and phreatic evaporations, were measured in the field. The first one was measured with evaporation pans, and the second one with lysimeters. Furthermore, a spatio-temporal analysis of the evaporation discharge, which included these measurements, was performed.

The zoning adopted for this study is shown in Fig. 5. This zoning considered the different types of soil reported by Mardones (1998) and the after modifications performed by Marazuela et al. (2019a).

#### 2.2.1. Evaporation from free water surface: evaporation pans

The evaporation rate in the free water surface was measured in three evaporation pans located in the nucleus and mixing zone (see their locations in Fig. 5). Evaporation pans were used to measure the water evaporating from a tank of regular dimensions. The Class A model of the U.S. National Weather Service was chosen for this purpose

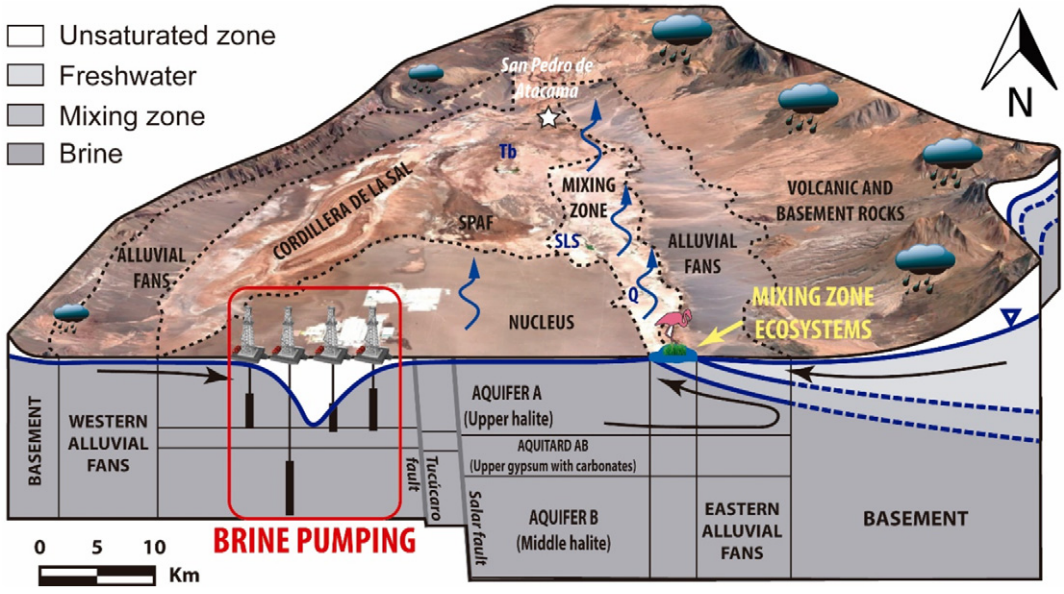


**Fig. 3.** Conceptual model of the Salar de Atacama basin. Q is Quelana Lake, SLS is the Soncor Lake System, Tb is Tebenquiche Lake and SPAF is the San Pedro alluvial fan. Black arrows show the groundwater flow movement direction.

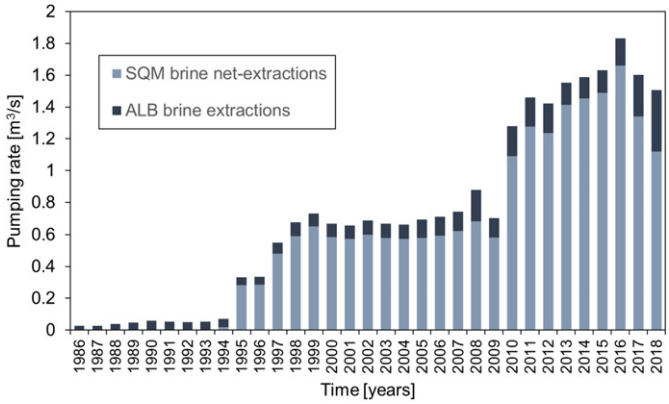


**Fig. 4.** Temporal evolution of the brine extractions in the Salar de Atacama. In the case of the SQM Company, the pumping rate consider the net value that is to say the brine pumping minus the reinjections from the evaporation ponds.

(Brutsaert, 1982) (Fig. 6A). Tanks were cylindrical in shape and were 120.65 cm in diameter and 25.4 cm deep. They were installed on a wooden platform, positioning the bottom of the tanks 10 cm above the surface of the soil to allow the flow of air below the tank. The tanks were filled with freshwater up to 5 cm from the top edge and were refilled when 2.5 cm of water had evaporated. The evaporation rate was estimated using a data logger that measured the water level oscillations. Because the dimensions of the tanks were known, the calculation of the evaporation rates was direct.

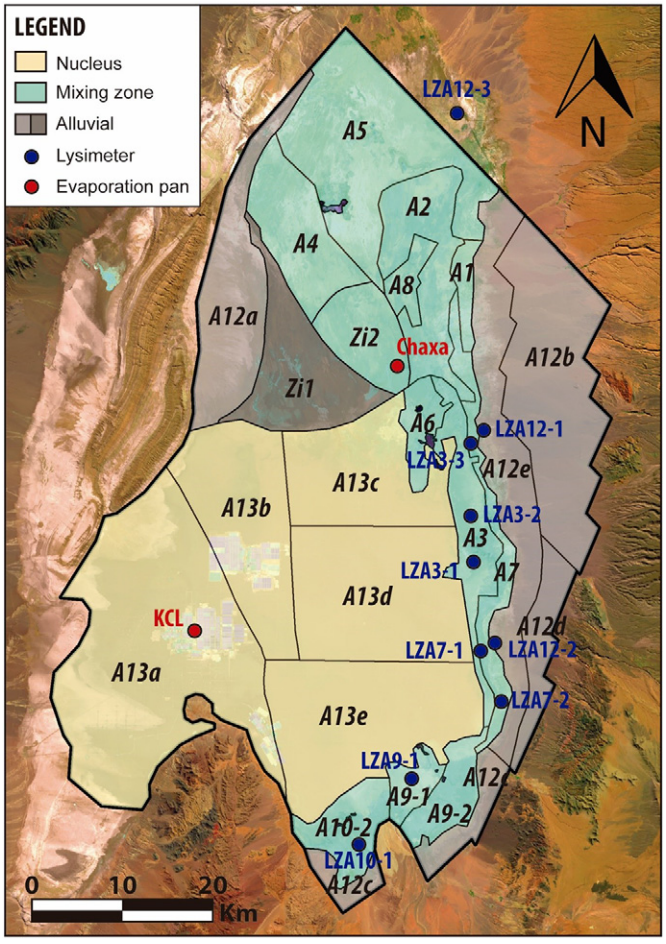


**Fig. 5.** Evaporation zoning of the Salar de Atacama basin. The locations of the pan evaporation and lysimeters are shown.

Measurements of pan evaporation ($E_p$) are, in general, greater than the potential evaporation ($E_0$) due to the characteristics of the instrumentation and the salinity of the water. The first limitation is compensated through an empirical correction coefficient known as the pan coefficient ($K_p$). This coefficient was estimated in previous works around 0.75 for the Salar de Atacama considering its climatic and environmental features (Dirección General de Aguas, 2014, 2010; HARZA, 1978). The salinity coefficient ($K_s$) accounts for the effect of salinity on the water activity (Obianyo, 2019). An annual average value of $0.94 \pm 0.02$ was calculated from major element concentration analysed in the Chaxa lagoon using the PHREEQC software and the *pitzer.dat* database (Parkhurst and Appelo, 2013). This value is close to 0.95 calculated from average salinity values (Ide, 1978). Therefore, the calculation of the potential evaporation was performed as follows:

$$E_0 = E_p \cdot K_p \cdot K_s \quad (1)$$

*2.2.2. Phreatic evaporation: lysimeters*

The measurement of the phreatic evaporation rate was carried out using 10 lysimeters (lysimeter locations are shown in Fig. 5). Lysimeters data corresponded to the period from August 2015 to June 2018. The lysimeters were distributed in order to occupy the largest possible area of the mixing zone, where the highest evaporation rates occur and the largest range of water table depths is currently available.

Each lysimeter is composed of two connected tanks buried in the ground (Fig. 6B). The first tank was filled with local water (water tank) and the second tank (soil tank) contained an unaltered soil sample to maintain the hydraulic characteristics under natural conditions. The water level in both tanks was the same because, when connected, the pressures were equalized. Evaporation from the ground occurred in the soil tank, and the level variations were measured by the pressure data logger installed in the water tank. The lysimeter measured the variation in the water level due to evaporation. Determining the level difference for a known time interval and considering the measurements of the water tank allowed us to calculate the volume of water that evaporated over this time interval; therefore, the evaporation rate was obtained.

For the estimation of the evaporation rate (E) with the water table depth, the methodology of Philip (1957) was adopted. This method correlates the evaporation rate measured at the surface with the water table depth through an exponential adjustment:

$$E = E_0 \cdot e^{(-b \cdot z)} \quad (2)$$

where $E_0$ is the potential evaporation from free water surface, z is the water table depth, and b is an adjustment parameter that was obtained by fitting the experimental data with the linearized form of the Eq. (2) via the Gnuplot 5.2 software (Williams and Kelley, 1986).

The data obtained of each lysimeter were plotted together representing the maximum variability. This variability was limited by adjusting the envelopes that represented the minimum and maximum evaporation values, similar to other works (Dirección General de Aguas, 2014, 1986; Johnson et al., 2009). The adjustment of each curve was performed by fitting the minimum, average and maximum values of the parameter b.

*2.2.3. Spatial analysis of the water table depth*

Two raster maps that represented the spatial distribution of water table depths and phreatic evaporation rates with a resolution of $200 \times 200$ m were performed for the years 1986 and 2018 to evaluate the temporal evolution of the discharge produced by phreatic evaporation in the Salar de Atacama basin. These two temporal snapshots represented, in the first case, the natural regime, prior to brine pumping and, in the second case, the current regime under brine exploitation.

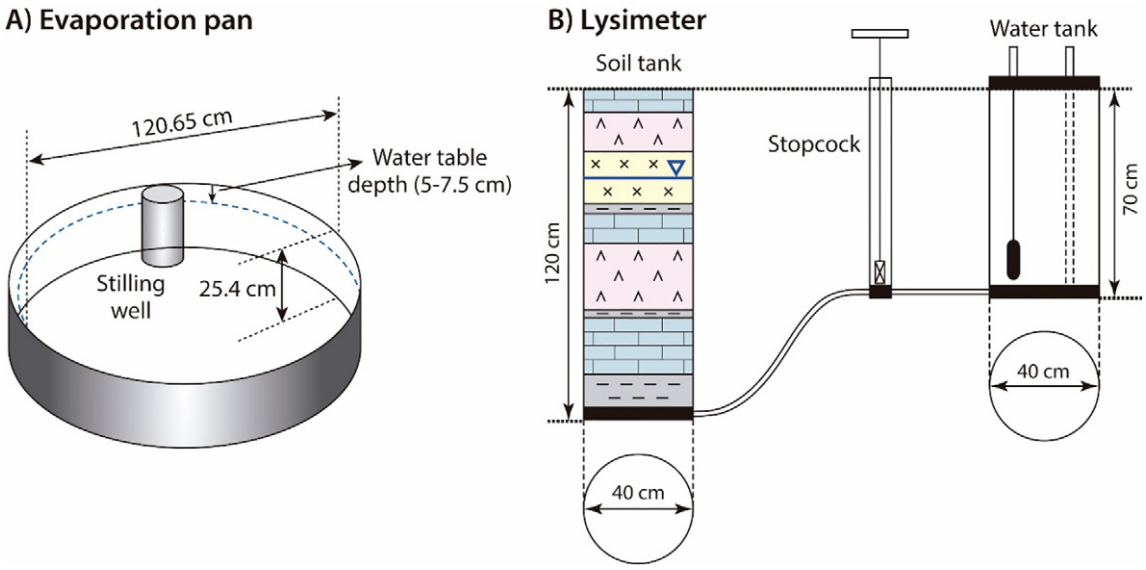


**Fig. 6.** Designs of the A) pan evaporation and B) lysimeter installed in the Salar de Atacama.

The hydraulic head data necessary to perform the water table depth raster were provided by the historical record of SQM S.A. and was complemented with data of Bevacqua (1988), Rio Chilex S.A. (1997), Golder Associates (2017a, 2017b) and Rockwood-Lithium (2015). The calculation of the water table depth from the hydraulic heads was conducted by considering the elevation of the ground. This elevation was measured in a topographic campaign with differential GPS due to the necessary precision and the difficulty of estimating ground elevation by satellite images as a consequence of the scarce topographic gradient and the irregularity of the salt crust. Moreover, control points in the lakes connected to the water table (water table depth equal to 0 m) and in the boundary of the domain were incorporated to properly inter- and extrapolate the measured data. A total of 1066 data points were considered for the 1986 raster, and 1816 data points for the 2018 raster, of which 60 and 401 data points, respectively, corresponded to direct measurements, 856 data points corresponded to boundary conditions in free water surface bodies each case and 53 and 31 data points, respectively, corresponded to the domain boundary to facilitate the extrapolation in the peripheral area. In the cases in which more than one data point was available, the average of the data was considered. The interpolation between data was performed using the natural neighbour method.

Once the water table depths were estimated for 1986 and 2018, the evaporation rates for both years were estimated. The local evaporation curves for each evaporation zone was fitted using Eq. (2) in which lysimeter data were available (zones A3, A7, A9-1, A9-2, A10-2 and A12). For the salt flat nucleus the mean values of lysimeters LZA3-2 and LZA3-3 were selected based on their proximity to the nucleus and soil characteristics. For the rest of the evaporation zones, the general evaporation curve resulting from the fitting of data from all lysimeters was used.

In addition, the sensitivity of the evaporation discharge to the water table depth accuracy was evaluated considering a gradual deepening of the water table until 0.5 m below the estimated water table for the years 1986 and 2018. The discharge from the lakes remained constant in all cases.

### 2.3. Numerical modelling

A synthetic parallelepiped model of 12,000 m of sides and 30 m of depth was performed to evaluate the improved brine exploitation design (Fig. 7). The model consisted of 6 layers with a total of 76,000 triangular prism elements and was considered a confined aquifer. The mesh was enough fine to avoid numerical oscillations and scale-effects. Finer meshes was evaluated to confirm the accuracy of the results. The hydraulic conductivity was 250 $m \cdot d^{-1}$ and the specific storage was $5 \cdot 10^{-3}$ $m^{-1}$. The FEFLOW code (Diersch, 2014) was used to solve the three-dimensional groundwater flow equation.

Six simulations were carried out considering three initial water table depths and two spatial distributions of the brine pumping wells. The simulations were run over 500 days. The outflows of the model were produced through the top as a consequence of the phreatic evaporation which was implemented using Eq. (1) and the fitting parameters of the nucleus of the Salar de Atacama. For the initial conditions, water table depths of 0, 0.2 and 0.4 m were considered. The inflows of the model were implemented in the bottom and corresponded with the phreatic evaporation value associated with the three different initial water table depths, with rates of 5.84, 2.15 and 0.79 $mm \cdot d^{-1}$ for the 0, 0.2 and 0.4 m depths, respectively. The sides of the model were considered as impervious.

The pumping was implemented with the well-type boundary condition and two extreme distributions were considered: (1) a single-well in the centre of the parallelepiped and (2) a regular network of multiple-wells with a separation distance of 4000 m. In the second case, the wells located in the sides and corners were analysed considering only a flow pumping of 50% and 25%, respectively. A total flow pumping rate of 2 $m^3 \cdot s^{-1}$ was implemented in slice 4 (15 m of depth) in both cases.

It is important to highlight that brine pumping is currently carried out in several hundred of wells in the Salar de Atacama based on the distribution of permeability and the lithium concentration (Houston et al., 2011). This numerical model seeks to quantify the effect and possible benefit of a decentralization of the pumps to consider it into future management plans of this or other salt flats.

## 3. Results and discussion

### 3.1. Evaporation rates in the Salar de Atacama

The measured values of the free water surface evaporation rates measured in the pans of KCL and Chaxa are shown in Fig. 8. The average value of pan evaporation was 8.2 $mm \cdot d^{-1}$ which after salinity and pan coefficient corrections was reduced to a potential evaporation rate of 5.84 $mm \cdot d^{-1}$. There was a marked seasonal oscillation, i.e., the maximum potential evaporation rates were recorded in the month of December (summer) and the minimum rates were recorded in the

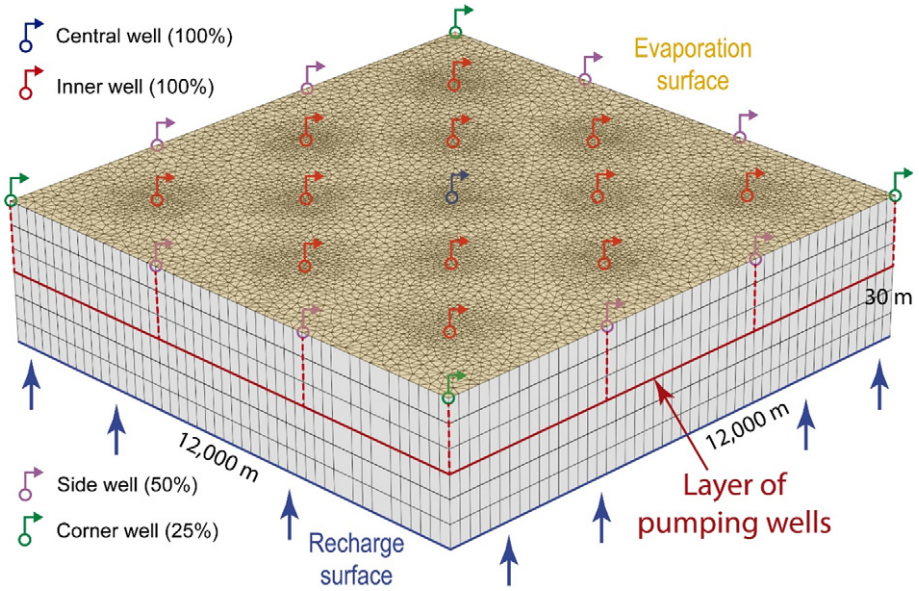


**Fig. 7.** Three-dimensional mesh of the synthetic model performed to study the efficiency of the brine exploitation in salt flats.

month of June (winter), with values ranging between 8.7 and 2.6 mm·d$^{-1}$, respectively. The historical series showed no trend of the average evaporation rate in the last two decades, so no impact of climate change on it was appreciated.

The local evaporation curves resulting from the adjustment of the lysimeter data are shown in Fig. 9. The measured data show a good fit through the Philip curve except for some anomalous values in the measures closest to the ground of the LZA3-3, LZA7-2 and LZA12-3 lysimeters. In these three lysimeters record, a data set values follows a vertical trend with depth which could be associated with residual measurement errors when evaporation rates are low. Furthermore, the Philips curve slightly undervalue the measured data for depths close to 0 m in LZA7-1, LZA9-1 and LZA12-1 cases, similar to the results obtained by Grilli and Vidal (1986). This suggests that the potential evaporation could be even slightly greater than the calculated and also an improvement of the Philip curve should be evaluated in future works. The general good agreement between calculated and observed data allows to confirm that the pan coefficient ($K_p$) adopted for the correction of the evaporation pan is within range. It is usually assumed that the pan coefficient can be as low as 0.35 in hyperarid climates close to cropping areas, depending on the wind speed and the distance of dry fallow (Doorenbos and Pruitt, 1975). However, a value of 0.75 was considered

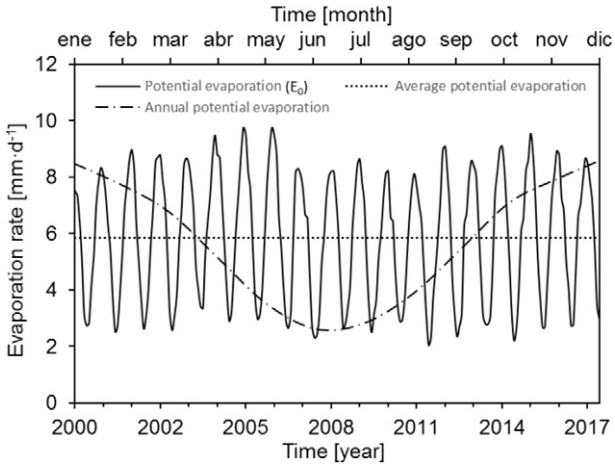


**Fig. 8.** Measurements of the potential evaporation in Chaxa and MOP evaporation pans.

a good approximation for the Salar de Atacama because crops are absent in the area and, moreover, lower values would further accentuate the undervaluation of evaporation rates when the water table is close to the ground surface leading to unrealistic estimations of the evaporation flow. Unlike surface evaporation, no clear seasonality was observed here in the measured data. Most of the exponential curves showed the strongest variability at water table depths between 0 and 0.5 m. In this range the evaporation rate decreased from 5.84 mm·d$^{-1}$ at 0 m to <1 mm·d$^{-1}$ at 0.5 m of depth. Only for lysimeter LZA9–1 the measured data showed an evaporation rate >1 mm·d$^{-1}$ at depths >0.5 m. This lysimeter was located in the "soft moderately rough crust" described by Kampf and Tyler (2006) which can explain its greater evaporation rates with respect to the other lysimeters that are located in or near "hard moderately rough crusts". At the other end, the lysimeter LZA3–2 showed the fastest reduction of the evaporation rate with the depth. In this case, the evaporation rate is close to extinction at only 0.3 m of depth which correspond to a very hard crust. In the rest of the lysimeters, the evaporation rates approached the extinction value at depths ranging between 0.5 and 1 m. According to these results, within the same type of soil (Kampf and Tyler, 2006) or zoning (Mardones, 1998) there is a high variability in the evaporation rate. This leads us to think that it is difficult to establish a homogenous evaporation curve for each zone possibly motivated by the fact that there are sharp contrasts of the soil type even within the same zone of defined soil type.

Due to the great variability of the measures and the unfeasibility of installing as many lysimeters as sub-types of soils exist, the set of all lysimeter data was used to build the general evaporation curve showed in Fig. 10. This general curve represents the maximum variability of the evaporation rate in the Salar de Atacama and may be of great interest when the local curve is not available or a general estimation of the evaporation is required. Because the dispersion is greater when considering a greater number of data, three fits were chosen similarly to (Johnson et al., 2009): lower, average and upper fit. The average fit match fairly well with the fit performed by Grilli and Vidal (1986) for the silt and sulphate crust (marginal zone). At depths very close to 0 m the undervaluation of their fit is higher than showed in the present work. This is mainly because the potential evaporation considered in the present work is higher than the adopted by these authors, 5.84 mm·d$^{-1}$ in front of 4.27 mm·d$^{-1}$. Even so, our adjustment still shows a certain undervaluation of the measured values, which can only be solved using the evaporation measured by the evaporation pans without applying

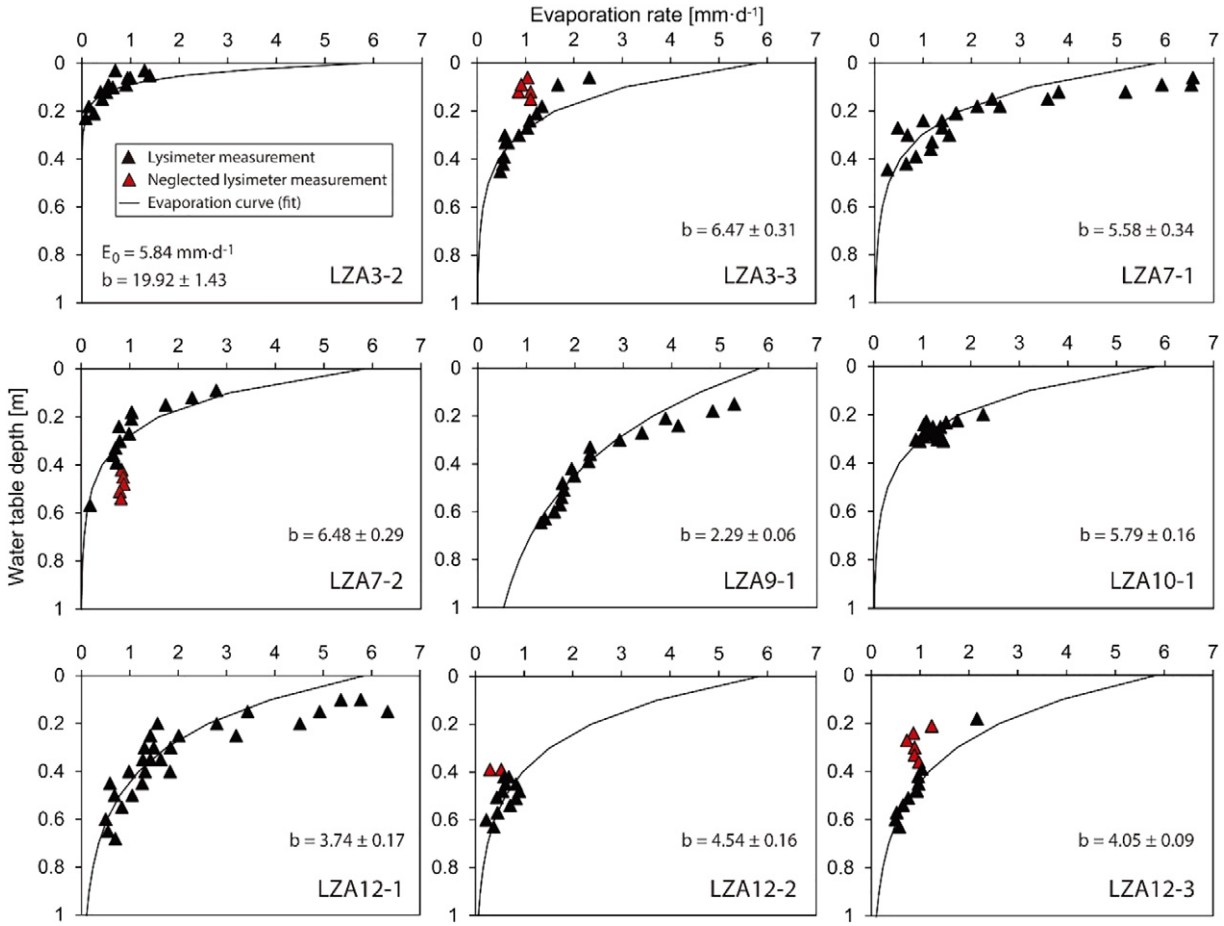


**Fig. 9.** Exponential relationship between evaporation rate and water table depth for each lysimeter (see their locations in Fig. 4). The data are given in Appendix A. The fit parameters and its error are shown.

correction (Fig. 10). Future work should explain this fact. The measurement performed by Grilli and Vidal (1986) pointed the minimum evaporation rate in the salt flat nucleus due to its hard crust. Furthermore, the fit performed for the salt flat nucleus and chloride crust by Grilli and Vidal (1986) is located between our average and lower fits. Summarizing, the average extinction depth at which evaporation can no longer occur may be established at 1 m, although in a conservative estimation this value could increases to 1.5–2 m considering the exception of lysimeter LZA9–1, or even reduces to 0.3 m considering the LZA3–2 lysimeter.

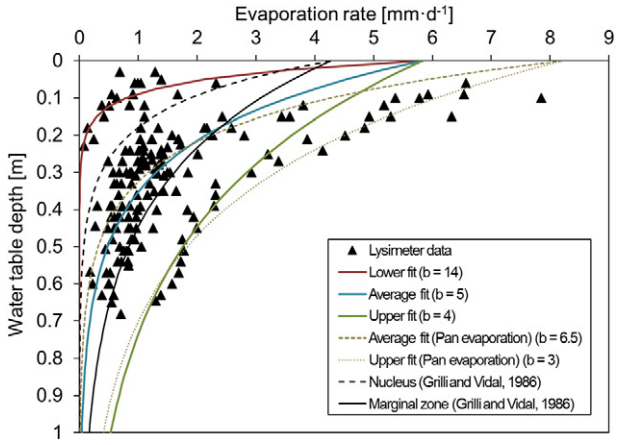


**Fig. 10.** General evaporation curve that shows the decreasing of the evaporation rate with the water table depth considering the total measurements. The fit parameter b is shown in parenthesis.

### 3.2. Evolution of the discharge by evaporation in the Salar de Atacama basin

The estimation of the evaporation discharge in the Salar de Atacama requires an accurate analysis of the water table depth besides the estimation of the evaporation rate performed in the previous section. Moreover, this spatial estimation needs to incorporate the temporal evolution of evaporation if determining the impacts of brine pumping on the evaporation discharge is an objective. In a first step, we perform a detailed spatial analysis of the water table depths which, subsequently, is used to quantify the spatial distribution of the evaporation discharge. These estimations were performed for both the natural regime prior to intensive brine pumping (year 1986) and the present regime under intensive brine pumping (year 2018) to quantify the impact in the water balance of the basin.

#### 3.2.1. Water table depth evolution from 1986 to 2018

The water table depths for the years 1986 and 2018 are shown in the rasters maps of the Fig. 11. In 1986, the mixing zone had water table depths shallower than 0.5 m. The salt flat nucleus showed depths ranging between deeper than 2 m on the western side, near the western alluvial fans, and shallower than 0.5 m on the eastern side, near the mixing zone. The northwestern and eastern alluvial fans had water table depths deeper than 2 m in all cases. However, when this water table depth distribution was compared with the present distribution (year 2018), important changes stand out in almost all areas (Fig. 12). At present, the water table depths in the northern mixing zone are

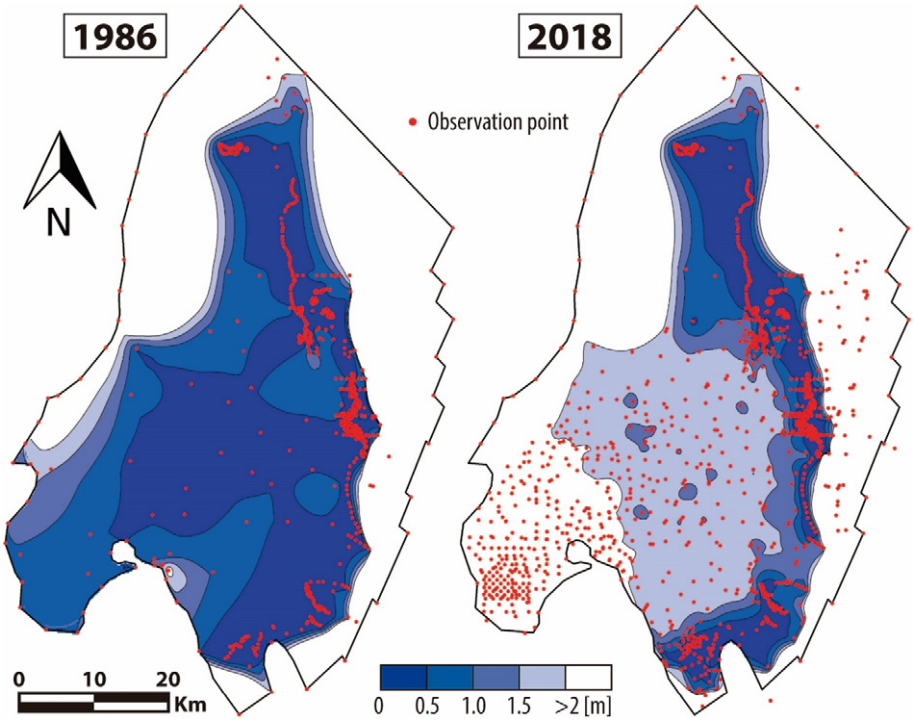


**Fig. 11.** Raster maps of the water table depth for the years 1986 and 2018.

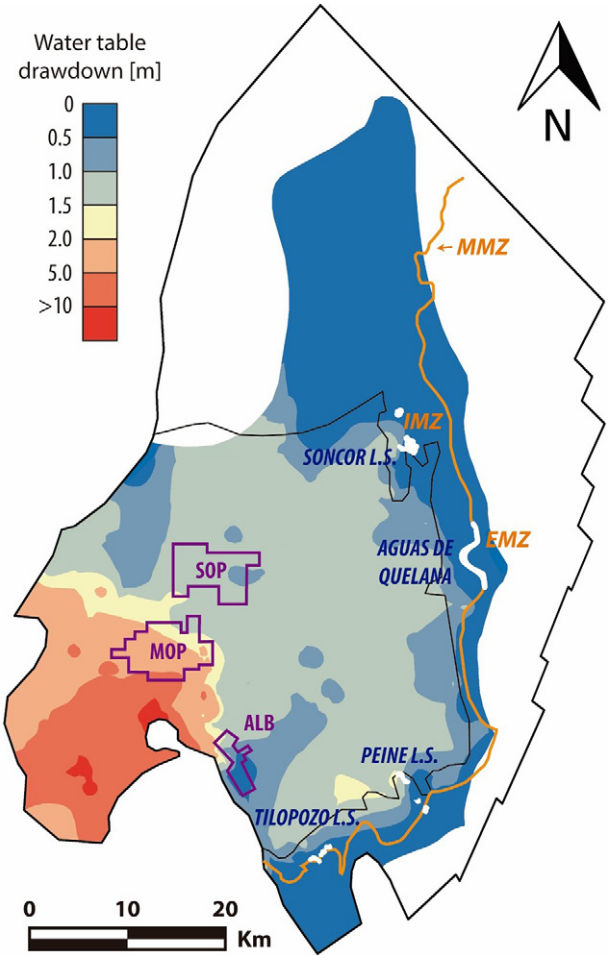


**Fig. 12.** Raster maps showing the drawdown evidenced in the Salar de Atacama from 1986 to 2018.

equivalent to the values in 1986. Something similar happens with the eastern and southeastern mixing zone where only a small increase in depth was identified locally. However, the salt flat nucleus was, quantitatively, the most affected area. The eastern salt flat nucleus evolved from water table depths shallower than 0.5 m in 1986 to depths below 1.5 m in 2018. The western salt flat nucleus had deeper water tables reaching depths below 2 m. This drawdown of the water table was caused by the brine pumping carried out in the south and southwest of the salt flat nucleus.

*3.2.2. Evaporation rates and water balance impacts*

The deepening of the water table has an indirect impact in the water balance of the basin as because the phreatic evaporation rate depends on the water table depth, as described above. Thus, the calculation of the evaporation rate for each pixel of the water table depth rasters considering the most adequate evaporation curve for each zone in 1986 and 2018, was performed (Fig. 13). The spatial distribution of the phreatic evaporation rates also permitted the accurate estimation of the discharge flows for each evaporation zone. These values are shown in Table 1 for 1986 and 2018.

The deepening of the water table caused a non-homogenous reduction in the evaporation rate of the salt flat basin. In the nucleus, prior to brine pumping, the average evaporation rate was approximately 0.03 $mm \cdot d^{-1}$. In 1986, the minimum evaporation rate, which had values close to 0 $mm \cdot d^{-1}$, occurred in the western area due to the relative high thickness of the unsaturated zone and near the ALB evaporation pond where early brine pumping had already started. The maximum evaporation rates in the nucleus were located near the Peine and Soncor Lake Systems, locally reaching values higher than 0.5 $mm \cdot d^{-1}$. After brine pumping, in 2018, almost the total area of the water table in the nucleus experienced a drawdown below the extinction depth. Only near the Peine and Soncor Lake Systems still some outflows remain at present. The drawdown in the nucleus led to a reduction of 96% of the evaporation flow that characterized the natural regime, resulting in an impact of 0.48 $m^3 \cdot s^{-1}$ in the water balance.

The evaporation rate in the mixing zone, in both periods, reached values of 5.84 $mm \cdot d^{-1}$ in the lakes and values <0.5 $mm \cdot d^{-1}$ in areas

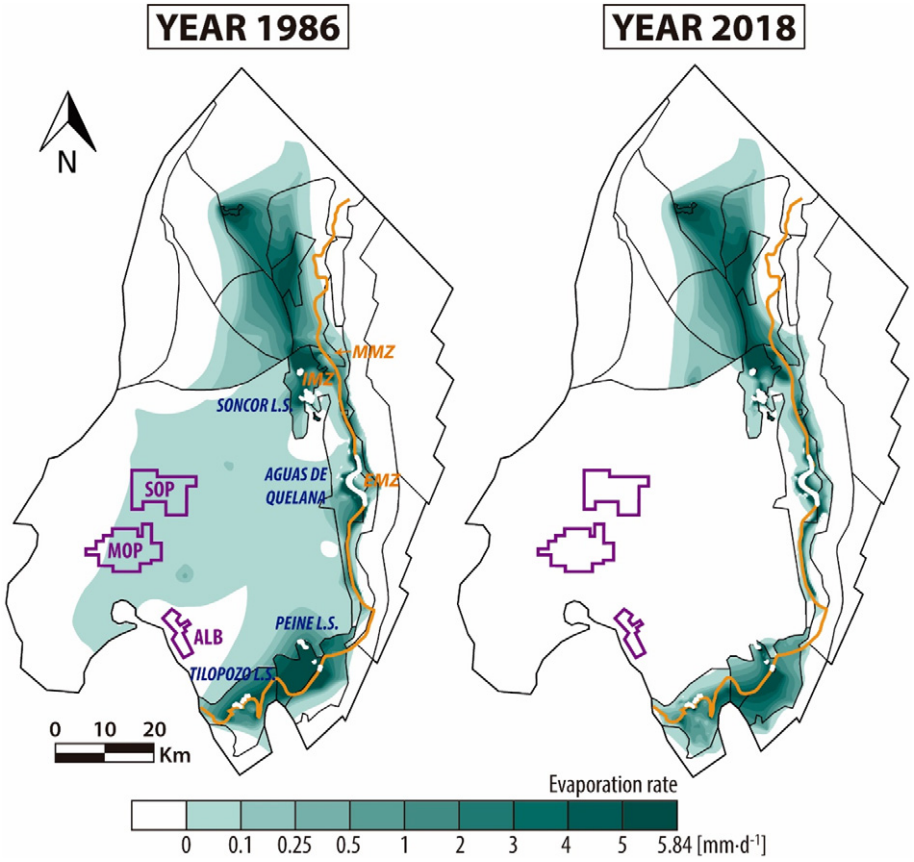


**Fig. 13.** Raster maps of the evaporation rates in 1986 and 2018.

**Table 1**
Evaporation discharge [$m^3 \cdot s^{-1}$] quantified for each evaporation zone of the Salar de Atacama (see Fig. 5 for the distribution of the evaporation zones) assuming an error of 0 to −0.5 m in the water table measurement.

| Domain | Zone | Calculated | | Error −0.1 [m] | | Error −0.2 [m] | | Error −0.3 [m] | | Error −0.4 [m] | | Error −0.5 [m] | |
|---|---|---|---|---|---|---|---|---|---|---|---|---|---|
| | | 1986 | 2018 | 1986 | 2018 | 1986 | 2018 | 1986 | 2018 | 1986 | 2018 | 1986 | 2018 |
| MIXING ZONE | A1 | **0.00** | **0.00** | 0.00 | 0.00 | 0.00 | 0.00 | 0.00 | 0.00 | 0.00 | 0.00 | 0.00 | 0.00 |
| | A2 | **1.38** | **1.80** | 0.88 | 1.18 | 0.58 | 0.80 | 0.40 | 0.58 | 0.29 | 0.44 | 0.23 | 0.35 |
| | A3 | **1.02** | **0.88** | 0.71 | 0.70 | 0.67 | 0.67 | 0.66 | 0.67 | 0.66 | 0.67 | 0.66 | 0.67 |
| | A4 | **0.13** | **0.12** | 0.08 | 0.08 | 0.05 | 0.05 | 0.03 | 0.03 | 0.02 | 0.03 | 0.02 | 0.02 |
| | A5 | **1.63** | **1.81** | 1.11 | 1.23 | 0.80 | 0.87 | 0.61 | 0.66 | 0.50 | 0.53 | 0.43 | 0.45 |
| | A6 | **1.17** | **0.96** | 0.92 | 0.83 | 0.77 | 0.76 | 0.67 | 0.71 | 0.62 | 0.68 | 0.59 | 0.67 |
| | A7 | **0.73** | **0.65** | 0.46 | 0.41 | 0.32 | 0.29 | 0.25 | 0.22 | 0.21 | 0.19 | 0.19 | 0.17 |
| | A8 | **1.04** | **0.88** | 0.78 | 0.68 | 0.62 | 0.56 | 0.52 | 0.48 | 0.46 | 0.44 | 0.43 | 0.41 |
| | A9–1 | **1.82** | **0.87** | 1.67 | 0.70 | 1.55 | 0.56 | 1.46 | 0.46 | 1.39 | 0.37 | 1.33 | 0.31 |
| | A9–2 | **0.96** | **1.32** | 0.82 | 1.11 | 0.72 | 0.94 | 0.63 | 0.81 | 0.56 | 0.71 | 0.51 | 0.62 |
| | A10 | **1.53** | **0.57** | 0.97 | 0.35 | 0.65 | 0.22 | 0.47 | 0.14 | 0.37 | 0.10 | 0.32 | 0.08 |
| | Zi2 | **1.09** | **0.97** | 0.68 | 0.61 | 0.43 | 0.39 | 0.28 | 0.25 | 0.19 | 0.17 | 0.13 | 0.12 |
| *Total mixing zone* | | ***12.49*** | ***10.82*** | *9.08* | *7.88* | *7.16* | *6.11* | *5.98* | *5.01* | *5.27* | *4.33* | *4.84* | *3.87* |
| ALLUVIAL | Zi1 | **0.09** | **0.06** | 0.06 | 0.04 | 0.03 | 0.02 | 0.02 | 0.01 | 0.01 | 0.01 | 0.01 | 0.00 |
| | A12a | **0.00** | **0.00** | 0.00 | 0.00 | 0.00 | 0.00 | 0.00 | 0.00 | 0.00 | 0.00 | 0.00 | 0.00 |
| | A12b | **0.00** | **0.00** | 0.00 | 0.00 | 0.00 | 0.00 | 0.00 | 0.00 | 0.00 | 0.00 | 0.00 | 0.00 |
| | A12c | **0.00** | **0.00** | 0.00 | 0.00 | 0.00 | 0.00 | 0.00 | 0.00 | 0.00 | 0.00 | 0.00 | 0.00 |
| | A12d | **0.00** | **0.00** | 0.00 | 0.00 | 0.00 | 0.00 | 0.00 | 0.00 | 0.00 | 0.00 | 0.00 | 0.00 |
| | A12e | **0.11** | **0.06** | 0.07 | 0.04 | 0.04 | 0.02 | 0.03 | 0.01 | 0.02 | 0.01 | 0.01 | 0.01 |
| *Total alluvial* | | ***0.20*** | ***0.12*** | *0.13* | *0.08* | *0.07* | *0.04* | *0.05* | *0.02* | *0.03* | *0.02* | *0.02* | *0.01* |
| NUCLEUS | A13a | **0.00** | **0.00** | 0.00 | 0.00 | 0.00 | 0.00 | 0.00 | 0.00 | 0.00 | 0.00 | 0.00 | 0.00 |
| | A13b | **0.00** | **0.00** | 0.00 | 0.00 | 0.00 | 0.00 | 0.00 | 0.00 | 0.00 | 0.00 | 0.00 | 0.00 |
| | A13c | **0.01** | **0.01** | 0.00 | 0.00 | 0.00 | 0.00 | 0.00 | 0.00 | 0.00 | 0.00 | 0.00 | 0.00 |
| | A13d | **0.01** | **0.00** | 0.00 | 0.00 | 0.00 | 0.00 | 0.00 | 0.00 | 0.00 | 0.00 | 0.00 | 0.00 |
| | A13e | **0.15** | **0.00** | 0.02 | 0.00 | 0.00 | 0.00 | 0.00 | 0.00 | 0.00 | 0.00 | 0.00 | 0.00 |
| *Total nucleus* | | ***0.16*** | ***0.01*** | *0.02* | *0.00* | *0.00* | *0.00* | *0.00* | *0.00* | *0.00* | *0.00* | *0.00* | *0.00* |
| TOTAL [$m^3 \cdot s^{-1}$] | | ***12.85*** | ***10.95*** | *9.23* | *7.96* | *7.23* | *6.15* | *6.03* | *5.03* | *5.30* | *4.35* | *4.86* | *3.88* |

near the nucleus and the alluvial fans where the thickness of the unsaturated zone increases. Considering the total area covered by the free water surface in the Salar de Atacama basin, an average evaporation flow of 0.24 $m^3 \cdot s^{-1}$ was obtained for the lakes. This value remained almost constant between both dates because the evaporation rate and the extension area covered by lakes remained almost constant. In the northern mixing zone, where the water table depth was fairly constant between 1986 and 2018, evaporation rates overall remained quite similar. In the eastern and southeastern mixing zones, the evaporation rate also remained constant in the EMZ and MMZ areas, but in the IMZ area, especially towards the nucleus side of this sub-zone, the slight drawdown of the water table caused a reduction in the evaporation rate. In percentage, the mixing zone experienced a minor reduction (14%) in the discharge flow than the nucleus, but this was enough to cause an impact in the evaporation flow of 1.78 $m^3 \cdot s^{-1}$, which was higher than the produced in the nucleus. Finally, the alluvial zone scarcely contributed to the water balance in 1986 and 2018 because the depth of the water table was always deeper than 2 m.

When the total evaporation discharge estimated for the year 1986, 13.38 $m^3 \cdot s^{-1}$, is compared with the evaporation flow calculated for the year 2018, 11.02 $m^3 \cdot s^{-1}$, a reduction of 2.36 $m^3 \cdot s^{-1}$, equivalent to 17%, is evidenced. This reduced flow is relatively similar to the flow pumped in recent years (Fig. 4), even somewhat higher. This means that the damping capacity has allowed practically all the brine that is pumped to be compensated with an equivalent reduction in evaporation. The water expelled by evaporation may be greater than the brine pumped because the estimation of the water table requires interpolating the water table depth data which adds a little uncertainty even though the data density is high. It can also influence the water table to be slightly above average as a result of a rainy period (Marazuela et al., 2019a). In 2018, part of the water that had been discharged naturally from the basin in 1986 was removed from the system by pumping. This possibly diminished the impact of the lakes and wetlands in the MMZ. From the MMZ to the boundary of the basin, the impact of brine pumping was seemingly almost null, even though the salt flat is a closed basin. It seems logical to conclude that the anthropogenic or natural exit of brine from the nucleus should not modify the hydraulic regime of the marginal zone as long as the amount of brine leaving the nucleus is the same. However, the damping capacity only works when the water table oscillates between the ground and the extinction depth (1–2 m) of the phreatic evaporation. In addition, the main damping capacity occurs in the first decimetres of depth, when the evaporation rate changes more rapidly. Below 0.5 m, due to the exponential change in the evaporation curve, the damping capacity is substantially reduced. The damping capacity played first in the nucleus, where the first drawdown of the water table occurred. However, as the extinction depth was reached, the damping capacity had ceased to be effective in the nucleus. This seems to be the current scenario. Our understanding of the system behaviour leads to think that the forward increase of the brine pumping and the drawdown caused in the water table suppose a potential risk to the lakes. In the case of the Soncor Lake System, the increase in the vertical hydraulic gradient could favour the infiltration from the lakes to the aquifer. To avoid or at least delay this regime as much as possible and to anticipate it, in the following section, we discuss one option of salt flat management through an improved distribution of wells.

#### 3.2.3. Sensitivity analysis

The strong dependence of the methodology followed for the estimation of the evaporation discharge on the water table depth implies that the accuracy of the water table measurement is critical. In addition, the low topographic gradient and the presence of a rough surface crust in salt flats hinders the elevation measurement of the ground.

The sensitivity analysis evaluated the impact of an error of 0.1 to 0.5 m in the water table on the evaporation rate for the years 1986 and 2018. In the most adverse scenario evaluated, assuming an error of −0.5 m and keeping constant the outflow from lakes, the evaporation discharge decreased from 12.85 and 10.95 $m^3 \cdot s^{-1}$ to 4.86 and 3.88 $m^3 \cdot s^{-1}$ for 1986 and 2018, respectively (Fig. 14 and Table 1). Thus, an error of only 0.5 m was enough to reduce in >60% the calculated evaporation discharge. The results confirmed the critical dependency of the evaporation discharge estimation to the water table depth accuracy. The accuracy of the groundwater level measurements and the evaporation zoning considered in each study have been the main reason why the historical estimations of the evaporation discharge in the Salar de Atacama have ranged between 1.6 $m^3 \cdot s^{-1}$ and 22.7 $m^3 \cdot s^{-1}$ (Kampf and Tyler, 2006; Marazuela et al., 2019a; Mardones, 1986). Therefore, despite the high efficiency of the methodology applied, it is critical to invest efforts in a sufficient number of observation wells and precise measurement of groundwater levels to accurately quantify the evaporation discharge of any salt flat.

### 3.3. Minimizing the impacts of brine pumping

The most efficient spatial-distribution of brine pumping wells to minimize the impact of pumping on the water balance and water table was determined using a 3D groundwater flow model. This numerical model reproduced a synthetic salt flat nucleus in which two extreme distributions of pumping wells, single- and multiple-wells extracting the same water flow were evaluated. The evaporation curve representative of the nucleus of the Salar de Atacama and similar to the evaporation curve of other salt flats (e.g. Grilli and Vidal, 1986) was incorporated in the top of the model to regulate the evaporation discharge as the water table is depleted by brine pumping. Furthermore, as not all salt flats have water tables at the same depth, three initial water table depths of 0.30, 0.15 and 0 m were considered. The depth of 0.3 m implied an initial evaporation rate of 0.10 $mm \cdot d^{-1}$ within the evaporation range of the Salar de Atacama in its natural regime (Fig. 15). The depth of 0 m represented an extreme case, in which the system would be a lake with an evaporation rate of 5.84 $mm \cdot d^{-1}$.

The initial evaporation rate was reduced depending on the distribution of the pumping wells (Fig. 15). In the multiple-wells case, several small cones of depression deepened the water table more homogeneously than in the single-well case, in which the brine pumped at one point caused a unique and deep cone of depression. This resulted in a different reduction in the evaporation rates. The reduction in the evaporation rate was more homogeneous and affected a greater area when the brine pumping was distributed in several wells than when brine pumping was conducted in a single-well (Fig. 15C). In the single-well case, the reduction in the evaporation rates was concentrated around the well, and far away, the evaporation rate remained close to the natural regime.

The temporal evolution of the evaporation rate reduction and the storage loss is shown in Fig. 16. In all cases, the initial evaporation rate was rapidly reduced as a result of the water table drawdown caused by the pumping. The new evaporation rate reached 0 $mm \cdot yr^{-1}$, i.e. the extinction depth, for the initial 0.15 and 0.30 depths. In these two cases, the reduction in the evaporation discharge could not compensate for the brine pumped and the extinction depth of the phreatic

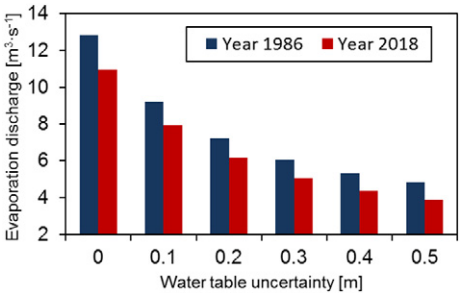


**Fig. 14.** Evaporation discharge values obtained from the sensitivity analysis of the water table accuracy.

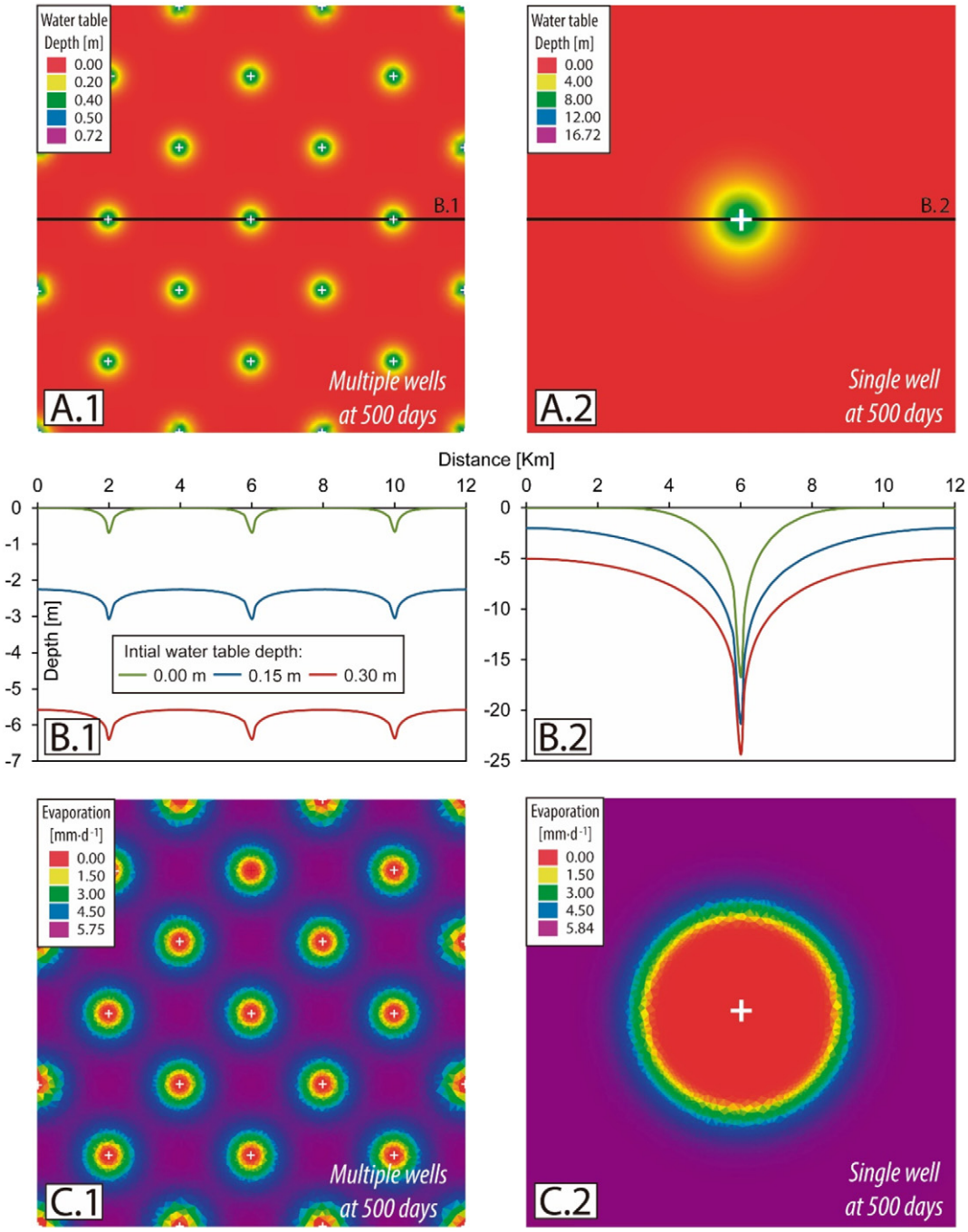


**Fig. 15.** Spatial distribution of the hydraulic heads and evaporation rates from the 3D numerical model. A) Hydraulic heads at 500 days. B) Hydraulic heads in the section at 500 days. Note the different vertical scales. The location of the section is shown in Fig. 15A. C) Evaporation rates at 500 days. The left three figures refer to the single-well design, and the right three figures refer to the multiple-wells design. The white crosses indicate the locations of the pumping wells.

evaporation was reached. For the initial water table depth of 0 m (lake case), the deepening of the water table allowed a reduction in the evaporation rate high enough to compensate for the brine pumped. Then, the new evaporation rate was equilibrated below the initial evaporation rate and above zero (Fig. 16). On the other hand, for each of the three initial depths, a difference in the evaporation rate between single- and multiple-well cases was clearly observed. The distribution of multiple-wells resulted in a faster decrease in evaporation, indicating a more efficient use of the damping capacity. In the case of the single-well, as the pumping was concentrated at one point, the extinction depth was quickly reached in the area closest to the pumping site, while in the most distant areas, the decrease in the evaporation rate was relatively slow.

Additionally, the changes in the evaporation rate had a direct impact on the storage of the aquifer and, as a consequence, on the stabilization of the water table. In all cases, the initial loss of storage coincided with the brine pumping of 2 $m^3 \cdot s^{-1}$, but this value immediately dropped until stabilizing concomitantly with the evaporation rate. This stabilization reached zero loss of storage in the 0 m depth case because the reduction in the initial evaporation rate allowed full compensation for the brine pumped. In the 0.3 and 0.15 m depth cases, as the evaporation rate reduction did not completely compensate for the brine pumped, the stabilization of the storage loss occurred when the phreatic evaporation stopped due to water table deepening. In these two cases, the water table continued to fall indefinitely because there was no longer any damping capacity. If this result is compared with the observations

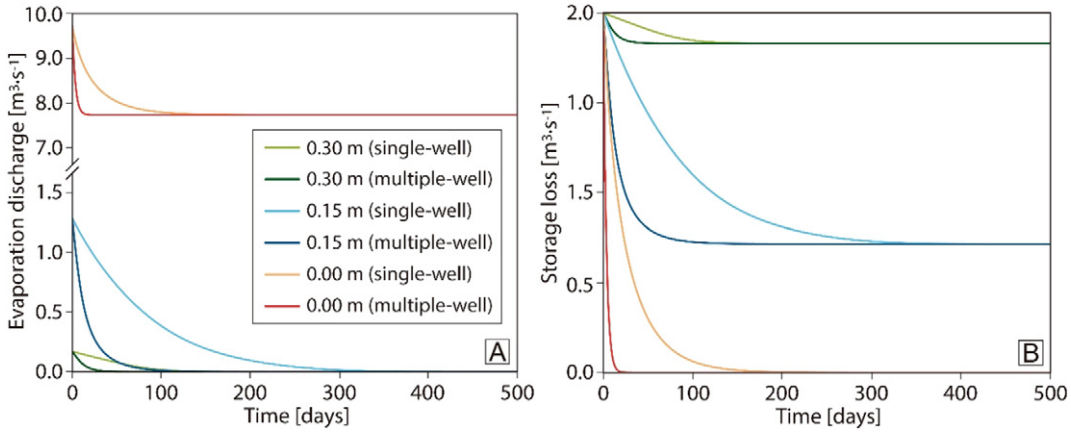


**Fig. 16.** Evaporation rates and storage resulting from the synthetic numerical model. A) Evolution of the total evaporation. B) Evolution of the storage.

performed in the nucleus of the Salar de Atacama, where the extinction depth of the phreatic evaporation has been already reached, the reduction in the evaporation rate will not be sufficient to compensate for the brine pumped.

While it is true that the difference between the two distributions of wells became null when the system stabilized, in a real case, the system will not reach stabilization, since the pumps are not constant over time and the recharge is neither constant nor homogeneous. Therefore, it is evident that the use of a multiple-wells system takes better advantage of the damping capacity of the water table and balance and the water table of salt flats than the use of a single-well system. In accordance with the results of these six simulations, the use of a multiple-wells design instead of a single-well design allowed to compensate for an extra of 65%, 33% and 5% of the pumped brine in the cases with initial water table depths of 0, 0.15 and 0.3 m, respectively. These percentages refer to the maximum storage difference between the single- and multiple-wells distributions with respect to the maximum storage ($2\ m^3 \cdot s^{-1}$). Furthermore, because the evaporation curve decreases exponentially with the water table depth, the more superficial the water table, the greater the damping capacity that is harnessed.

## 4. Synthesis and conclusions

The methodology proposed to quantify the evaporation discharge in the Salar de Atacama and to evaluate the impacts caused by its brine exploitation allowed to improve the design of the brine exploitation in salt flats. The methodology included (1) field measurements of water table and evaporation rate, (2) its spatio-temporal analysis and (3) numerical modelling to improve the brine exploitation design.

First, evaporation pans and lysimeters were used to measure the evaporation rates from the free water surface of lakes and the phreatic evaporation, respectively. The potential evaporation rate was estimated in $5.84\ mm \cdot d^{-1}$. The lysimeter measurements allowed to define the exponential decrease of the evaporation with respect to the water table depth. The strongest decrease occurred in the 0.5 m closest to the ground and the extinction of the evaporation was usually reached at 1 m of depth.

Second, the quantification of the evaporation discharge for the year 1986, prior to brine pumping, and 2018, under intensive brine extraction, was carried out through spatio-temporal analysis of the water table depth and the evaporation rate measurements. The evaporation discharge decreased from 12.85 to 10.95 $m^3 \cdot s^{-1}$ between 1986 and 2018 that is around 15%. This reduction compensated part of the extractions and could contribute to the preservation of the mixing zone ecosystems. The damping capacity was more efficient at water table depths between 0 and 0.5 m where the evaporation experienced the strongest decrease. At present, the damping capacity of the salt flat nucleus is already amortized. The sensitivity analysis showed that an average error of the water table depth of 0.5 m is enough to reduce the evaporation discharge of the basin by >60%. The sensitivity of the phreatic evaporation on the water table imposes that considerable effort should invested to faithfully quantify the discharge by evaporation which is critical in the water balance of the salt flat basins.

Third, the 3D groundwater flow model of a hypothetical salt flat under brine exploitation allowed to optimize the designs for the pumping wells in terms of water balance impact. The results showed that the damping capacity can reach to compensate the total pumped brine through a reduction of the initial evaporation discharge as a consequence of the water table drawdown. To take better advantage of the damping capacity and to minimize impacts on the water balance and water table, brine exploitations should consider to distribute the pumping outflow in the largest possible area.

Supplementary data to this article can be found online at https://doi.org/10.1016/j.scitotenv.2019.135605.

## Declaration of competing interest

The authors declare that they have no known competing financial interests or personal relationships that could have appeared to influence the work reported in this paper.

## Acknowledgments

The authors acknowledge Sociedad Química y Minera de Chile S.A. for their support and sharing data throughout the hydrogeological characterization of the Salar de Atacama site. M.A. Marazuela gratefully acknowledges the financial support from the AGAUR (Agència de Gestió d'Ajuts Universitaris i de Recerca, Generalitat de Catalunya) and the European Union (grant number 2017FI B1 00194).

## References

Acosta, O., Custodio, E., 2008. Impactos ambientales de las extracciones de agua subterranea en el Salar del Huasco (norte de Chile). Bol. Geol. y Min. 119, 33–50.
Arriagada, C., Cobbold, P.R., Roperch, P., 2006. Salar de Atacama basin: a record of compressional tectonics in the central Andes since the mid-Cretaceous. Tectonics 25, TC1008. https://doi.org/10.1029/2004TC001770.
Bevacqua, P., 1988. Descripción de las unidades geológicas de superficie del Salar de Atacama.
Boutt, D.F., Hynek, S.A., Munk, L.A., Corenthal, L.G., 2016. Rapid recharge of fresh water to the halite-hosted brine aquifer of Salar de Atacama, Chile. Hydrol. Process. 30, 4720–4740. https://doi.org/10.1002/hyp.10994.
Brutsaert, W., 1982. Evaporation Into the Atmosphere: Theory, History and Applications. Springer, Netherlands https://doi.org/10.1038/scientificamerican12121863-370.
Corenthal, L.G., Boutt, D.F., Hynek, S.A., Munk, L.A., 2016. Regional groundwater flow and accumulation of a massive evaporite deposit at the margin of the Chilean Altiplano. Geophys. Res. Lett. 43, 8017–8025. https://doi.org/10.1002/2016GL070076.
Diersch, H.-J.G., 2014. FEFLOW: Finite Element Modeling of Flow, Mass and Heat Transport in Porous and Fractured Media. https://doi.org/10.1007/978-3-642-38739-5.
Dirección General de Aguas, 1986. Balance Hidrologico Nacional II Region (Santiago, Chile).

Dirección General de Aguas, 2010. Actualización de la evaluación de la disponibilidad de recursos hídricos para constituir derechos de aprovechamientos en las subcuencas afluentes al Salar de Atacama. II Región Informe final (Santiago, Chile).
Dirección General de Aguas, 2013. Análisis de la oferta hídrica del Salar de Atacama (Santiago, Chile).
Dirección General de Aguas, 2014. Análisis de los mecanismos de evaporación y evaluación de los recursos hídricos del Salar de Atacama.
Doorenbos, J., Pruitt, W.O., 1975. Guidelines for predicting crop water requirements. Irrigation and Drainage Paper 24. Food and Agriculture Organization of the United Nations, Rome, p. 179.
Evans, R.K., 1978. Lithium reserves and resources. Energy 3, 379–385.
Flexer, V., Baspineiro, C.F., Galli, C.I., 2018. Lithium recovery from brines: a vital raw material for green energies with a potential environmental impact in its mining and processing. Sci. Total Environ. 639, 1188–1204. https://doi.org/10.1016/j.scitotenv.2018.05.223.
Golder Associates, 2017a. Informe nº16 Plan de Alerta Temprana para el acuífero Monturaqui-Negrillar-Tilopozo.
Golder Associates, 2017b. Modelo hidrogeológico conceptual y numérico para el acuífero de Monturaqui-Negrillar-Tilopozo.
González, G., Cembrano, J., Aron, F., Veloso, E.E., Shyu, J.B.H., 2009. Coeval compressional deformation and volcanism in the central Andes, case studies from northern Chile (23°S-24°S). Tectonics 28, 1–18. https://doi.org/10.1029/2009TC002538.
Grilli, A., 1985. Una aproximación al estudio de la evaporación desde salares. VII Congreso de Ingeniería Hidráulica.
Grilli, A., Vidal, F., 1986. Evaporación desde salares: metodología para evaluar los recursos hídricos renovables. Aplicación a las regiones I y II. Rev. la Soc. Chil. Ing. Hidráulica.
Hardie, L.A., 1991. On the significance of evaporites. Annu. Rev. Earth Planet. Sci. 19, 131–168.
HARZA, 1978. Desarrollo de los recursos de agua en el Norte Grande, Chile. United Nations (UN).
Houston, J., 2006. Evaporation in the Atacama Desert: an empirical study of spatio-temporal variations and their causes. J. Hydrol. 330, 402–412. https://doi.org/10.1016/j.jhydrol.2006.03.036.
Houston, J., Butcher, A., Ehren, P., Evans, K., Godfrey, L., 2011. The evaluation of brine prospects and the requirement for modifications to filing standards. Econ. Geol. 106, 1125–1239. https://doi.org/10.2113/econgeo.106.7.1225.
IDAEA-CSIC, 2017. Cuarta actualización del modelo hidrogeológico del Salar de Atacama (Accessed by permision).
Ide, F., 1978. Cubicación del yacimiento Salar de Atacama. Universidad de Chile.
Ide, F., Kunasz, I.A., 1990. Origin of lithium in Salar de Atacama, Northern Chile. In: Ericksen, G.E., Cañas-Pinochet, M.T., Reinemund, J.A. (Eds.), Geology of the Andes and Its Relation to Hydrocarbon and Mineral Resources, p. 452 Houston, Texas.
Johnson, E., Yáñez, J., Ortiz, C., Muñoz, J., 2009. Evaporation from shallow groundwater in closed basins in the Chilean Altiplano. Hydrol. Sci. J. 55, 624–635. https://doi.org/10.1080/02626661003780458.
Jordan, T.E., Mpodozis, C., Muñoz, N., Blanco, N., Pananont, P., Gardeweg, M., 2007. Cenozoic subsurface stratigraphy and structure of the Salar de Atacama Basin, northern Chile. J. S. Am. Earth Sci. 23, 122–146. https://doi.org/10.1016/j.jsames.2006.09.024.
Kampf, S.K., Tyler, S.W., 2006. Spatial characterization of land surface energy fluxes and uncertainty estimation at the Salar de Atacama, Northern Chile. Adv. Water Resour. 29, 336–354. https://doi.org/10.1016/j.advwatres.2005.02.017.
Kampf, S.K., Tyler, S.W., Ortiz, C.A., Muñoz, J.F., Adkins, P.L., 2005. Evaporation and land surface energy budget at the Salar de Atacama, Northern Chile. J. Hydrol. 310, 236–252. https://doi.org/10.1016/j.jhydrol.2005.01.005.
Kesler, S.E., Gruber, P.W., Medina, P.A., Keoleian, G.A., Everson, M.P., Wallington, T.J., 2012. Global lithium resources: relative importance of pegmatite, brine and other deposits. Ore Geol. Rev. 48, 55–69. https://doi.org/10.1016/j.oregeorev.2012.05.006.
Liu, W., Agusdinata, D.B., Myint, S.W., 2019. Spatiotemporal patterns of lithium mining and environmental degradation in the Atacama Salt Flat, Chile. Int. J. Appl. Earth Obs. Geoinf. 80, 145–156. https://doi.org/10.1016/j.jag.2019.04.016.
Lowenstein, T.K., Risacher, F., 2009. Closed basin brine evolution and the influence of Ca-Cl inflow waters: death valley and Bristol Dry Lake California, Qaidam Basin, China, and Salar de Atacama, Chile. Aquat. Geochemistry 15, 71–94. https://doi.org/10.1007/s10498-008-9046-z.
Marazuela, M.A., Vázquez-Suñé, E., Custodio, E., Palma, T., García-Gil, A., Ayora, C., 2018. 3D mapping, hydrodynamics and modelling of the freshwater-brine mixing zone in salt flats similar to the Salar de Atacama (Chile). J. Hydrol. 561, 223–235. https://doi.org/10.1016/j.jhydrol.2018.04.010.
Marazuela, M.A., Vázquez-Suñé, E., Ayora, C., García-Gil, A., Palma, T., 2019a. Hydrodynamics of salt flat basins: the Salar de Atacama example. Sci. Total Environ. 651, 668–683. https://doi.org/10.1016/j.scitotenv.2018.09.190.
Marazuela, M.A., Vázquez-Suñé, E., Ayora, C., García-Gil, A., Palma, T., 2019b. The effect of brine pumping on the natural hydrodynamics of the Salar de Atacama: the damping capacity of salt flats. Sci. Total Environ. 654, 1118–1131. https://doi.org/10.1016/j.scitotenv.2018.11.196.
Mardones, L., 1986. Características geológicas e hidrogeológicas del Salar de Atacama. In: Lagos, G. (Ed.), El Litio, Un Nuevo Recurso Para Chile, pp. 181–216.
Mardones, L., 1998. Flux et évolution des solutions salines dans les systèmes hydrologiques des salars d'Ascotan et d'Atacama. University of Paris.
Munk, L.A., Hynek, S.A., Bradley, D., Boutt, D.F., Labay, K., Jochens, H., 2016. Lithium brines: a global perspective. Rev. Econ. Geol. 18, 339–365.
Muñoz, N., Charrier, R., Jordan, T., 2002. Interactions between basement and cover during the evolution of the Salar de Atacama Basin, northern Chile. Rev. geológica Chile 29, 3–29. https://doi.org/10.4067/S0716-02082002000100004.
Muñoz-Pardo, J.F., Ortiz-Astete, C.A., Mardones-Pérez, L., de Vidts-Sabelle, P., 2004. Funcionamiento hidrogeológico del acuífero del núcleo del salar de Atacama, Chile. Ing. Hidráulica en Mex. XIX, 69–81.
Obianyo, J.I., 2019. Effect of salinity on evaporation and the water cycle. Emerg. Sci. J. 3, 255–262. https://doi.org/10.28991/esj-2019-01188.
Ortiz, C., Aravena, R., Briones, E., Suárez, F., Tore, C., Muñoz, J.F., 2014. Sources of surface water for the Soncor ecosystem, Salar de Atacama basin, northern Chile. Hydrol. Sci. J. 59, 336–350. https://doi.org/10.1080/02626667.2013.829231.
Parkhurst, D.L., Appelo, C.A.J., 2013. Description of input and examples for PHREEQC version 3—a computer program for speciation, batch-reaction, one-dimensional transport, and inverse geochemical calculations. Techniques and Methods. 6, p. 519.
Philip, J.R., 1957. Evaporation, and moisture and heat fields in the soil. J. Meteorol. 14, 354–366. https://doi.org/10.1175/1520-0469(1957)014<0354:EAMAHF>2.0.CO;2.
Rio Chilex S.A., 1997. Evaluación hidrogeológica acuífero sector norte Salar de Atacama.
Risacher, F., Alonso, H., Salazar, C., 2003. The origin of brines and salts in Chilean salars: a hydrochemical review. Earth-Science Rev 63, 249–293. https://doi.org/10.1016/S0012-8252(03)00037-0.
Rissmann, C., Leybourne, M., Benn, C., Christenson, B., 2015. The origin of solutes within the groundwaters of a high Andean aquifer. Chem. Geol. 396, 164–181. https://doi.org/10.1016/j.chemgeo.2014.11.029.
Rockwood-Lithium, 2015. Estudio Hidrogeológico y Modelo Numérico Sector Sur del Salar de Atacama (Anexo 1). Para Estudio de Impacto Ambiental Proyecto Modificaciones y Mejoramiento del Sistema de Pozas de Evaporación solar en el Salar de Atacama (Santiago, Chile).
Scheihing, K., Tröger, U., 2018. Local climate change induced by groundwater overexploitation in a high Andean arid watershed, Laguna Lagunillas basin, northern Chile. Hydrogeol. J. 26, 705–719. https://doi.org/10.1007/s10040-017-1647-4.
Tejeda, I., Cienfuegos, R., Muñoz, J.F., Durán, M., 2003. Numerical modeling of saline intrusion in Salar de Atacama. J. Hydrol. Eng. 8, 25–34. https://doi.org/10.1061/(ASCE)1084-0699(2003)8:1(25).
Vásquez, C., Ortiz, C., Suárez, F., Muñoz, J.F., 2013. Modeling flow and reactive transport to explain mineral zoning in the Atacama salt flat aquifer, Chile. J. Hydrol. 490, 114–125. https://doi.org/10.1016/j.jhydrol.2013.03.028.
Warren, J.K., 2010. Evaporites through time: tectonic, climatic and eustatic controls in marine and nonmarine deposits. Earth-Science Rev 98, 217–268. https://doi.org/10.1016/j.earscirev.2009.11.004.
Williams, T., Kelley, C., 1986. Gnuplot v5.2: An Interactive Plotting Program.
Yechieli, Y., Wood, W.W., 2002. Hydrogeologic processes in saline systems: playas, sabkhas, and saline lakes. Earth-Science Rev 58, 343–365. https://doi.org/10.1016/S0012-8252(02)00067-3.